# Engineering Design of Thermo-Magnetic Generator using Multi-objective Genetic Algorithm

Will Hintlian*, Hanfeng Zhai†
*Sibley School of Mechanical and Aerospace Engineering, Cornell University, Ithaca, NY*

Mads Peter Berg‡
*Applied and Engineering Physics, Cornell University, Ithaca, NY*
*Department of Physics, Technical University of Denmark, Lyngby, Denmark*

**Novel clean and green energy technologies are in strong demand as the world moves towards sustainability. Recovering waste heat is a step in the right direction, but very few technologies can convert low-grade waste heat into electricity. The so-called *thermo-magnetic generator* is one. Here, we present efforts undertaken in designing and optimizing a thermo-magnetic generator (TMG), using a multi-objective genetic algorithm (GA) and other approaches. Our optimization has been of a simple structure with the basic design scheme denoted, *genus 1*, (by Waske *et al*., *Nat. Energy*, 2019), where the structure is variant only in two dimensions. The optimization objectives are cost, power output, and the energy efficiency of the TMG, with the geometric quantities of heights and the widths of different parts as input design variables. The parameters are the physical properties, i.e., magnetic permeability, thermal diffusivity, etc., of the different parts and the ambient air as well as the operating settings, i.e., when to start and stop heating the *active material*, which we have not been considering the optimization of. Single objective optimization was applied to cost, power output, and efficiency, which provided us with three different designs. The effects of each design variable were also estimated, indicating that the "width of the gap" is the most effective factor for cost. Multi-objective optimization was applied to both cost, power output, and efficiency. It is found that using a genetic algorithm, worked significantly better for this particular problem, than a gradient-based one. We eventually present a suggested design as the TMG with the highest power per cost, generated from the multi-objective optimization. These studies can all provide guidelines and insights for future TMG design.**

## I. Nomenclature

| | | | | | |
|---|---|---|---|---|---|
| $w_{yk}$ | = | yoke width | $R$ | = | resistance |
| $h_{yk}$ | = | yoke height | $N$ | = | number of loops |
| $h_A$ | = | active material height | $\varepsilon$ | = | induced voltage |
| $h_{pm}$ | = | permanent magnet height | $t$ | = | time |
| $w_{gap}$ | = | gap width | $V$ | = | voltage |
| $P$ | = | power output | $I$ | = | magnetic current |
| $K$ | = | reparameterization multiplier | $T$ | = | temperature |
| $\eta$ | = | efficiency | $C_V$ | = | heat capacity |
| $\Phi$ | = | magnetic flux | $G$ | = | proportionality constant |

## II. Introduction

Efficient conversion of low-grade heat into useful power is a challenge [1]. There is an increasing focus on and investment in renewable energy like wind power [2], electrochemical energy [3], nuclear power [4], and many

*Email: wth42@cornell.edu
†Email: hz253@cornell.edu
‡Email: mpb99@cornell.edu

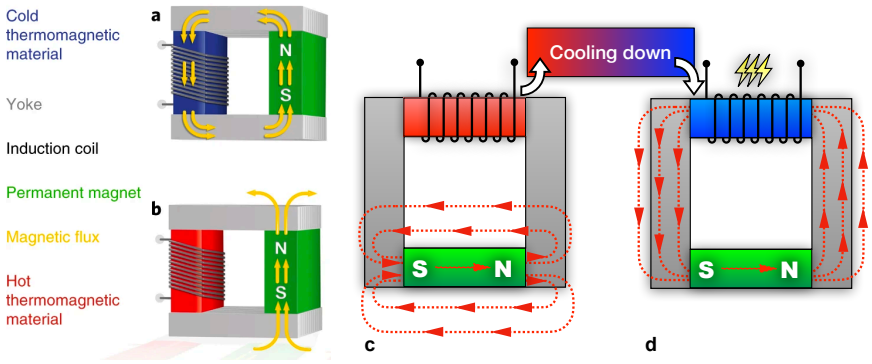


**Fig. 1 The schematic illustration of a thermo-magnetic generator. Note that subfigures a and b are reproduced from Waske *et al.* [5]. Subfigures c to d represents how the cooling down of the active magnetic materials generates electric power. Note that the red and blue indicates the temperature change on the active material which causes change in the magnetic permeability, generating electricity.**

related clean energies to substitute traditional fossil fuels. Industrial processes, residential heating, and not least vehicles, generate waste heat of very low-grade, but can be converted to useful energy [5] using non-traditional means, whereas heat engines can not be applied efficiently when the temperature differences are not large enough. A recent analysis reveals that the amount of global waste heat peaks just above room temperature [8]. Between 330 K and 390 K alone, this energy amounts to more than 3,500 PJ per year within the European Union alone [8]. The United States' industrial sector uses heat for a wide variety of applications, whose uses altogether are estimated at 24 quadrillion Btu, or roughly one-third of the nation's delivered energy supply [9]. In general, the drive towards improving electricity transmission efficiency and the replacement of oil-based fuels by electric motors in transportation technologies has motivated researchers to focus on magnetic material technologies [10]. Physics tells us that changes in a magnetic field can generate electricity, and the energy from this could go far in supporting our daily needs [11]. Employing this idea, the thermo-magnetic generator can convert waste heat into electricity as a form of clean energy. The technology can be traced back to more than 100 years ago, to Tesla [6] and Edison [7]. Here, we focus on the design of the TMG and employ a multidisciplinary design optimization (MDO) approach with the goal of producing an industrially satisfactory system design.

In our basic setup, we adopt Waske *et al.*'s approach [5], by modeling the TMG in 2D and studying it through the use of multiphysical simulation. The TMG is consisting of a permanent magnetic at the bottom, two *"yokes"* made of soft irons on the two sides, and active material on the top to generate electrical energy, as shown in Figure 1: the change of temperature in the active material will cause a change in the magnetic permeability of the active material and as a result, a phenomena will occur, where the "ability to guide a magnetic field" is changed. Intuitively, this can be understood such that the permanent magnet supplies a "source" of magnetic field lines and when the magnetic field is thus guided in and out of the active material as the magnetic permeability changes with temperature [13], a changing magnetic flux will be observed in the active material. This means that we can heat up and cool down the active material alternately and thus produce a time-dependent change in magnetic flux . Through the magic of electromagnetic induction, this can be used to produce a current in a coil wrapped around the active material, which is what we imagine that we have. The yoke is simply there to help guide the flux from the permanent magnet and to the active material. In this project, the active material is made out of Gadolinium. The permanent magnet is taken to be a Neodymium one, and the yoke is taken to be made of non-magnetized iron. The physical parameters of the simulation are based on this, as well as on the surroundings being air at 300K. For reference on how the magnetic permeability changes with temperature, see Ref. [19].

The geometric variables to be optimized will be the widths and heights of the different parts of the device, shown in this schematic Figure 2. As the number of studies on TMG's and related systems are relatively few, it is hard to benchmark the simulated results with real-world experimental ones. Moreover, the sparsity of the number of studies in this field indicates that applying MDO to computer simulation for suggested design could be meaningful since in such a way, it strongly reduces expenses compared with the traditional design optimization method: trying out numerous TMG designs to manufacture and propose a new design with empirical sense. The 2D numerical simulation of a TMG was carried out using COMSOL Multiphysics®. We also adopt MATLAB® for our genetic algorithm optimization. The

| Design variables | Modules | Description | Lower bounds | Nominal | Upper bounds |
|---|---|---|---|---|---|
| $w_{yk}$ | All | Yoke Width | 0.01 | 0.05 | 0.5 |
| $h_{yk}$ | All | Yoke Height | 0.01 | 0.4 | 0.5 |
| $h_A$ | All | Active Material Height | 0.01 | 0.1 | 0.5 |
| $h_{pm}$ | All | Permanent Magnet Height | 0.01 | 0.1 | 0.5 |
| $w_{gap}$ | All | Gap Width | 0.01 | 0.15 | 0.5 |

**Table 1 The design variables used for optimizing the TMG structure.**

optimization loop was automated through Livelink™.

The paper is arranged as followed: In Section III we formulate our MDO problem for the TMG by introducing our objectives, design variables, parameters, and constraints. In Section IV we present the physical model involved in the numerical simulation of the TMG, briefly estimate one of the simulation results from a random design, and benchmark the scale of the simulation with the work by Waske *et al.*, where the magnetic flux density in our simulation is $\sim$ 1T, same as in Fig. 3. c, Ref. [5]. Later in Section V we first briefly summarize the selection of the genetic algorithm (GA) and briefly explain why we apply it to the design of the TMG instead of gradient-based methods. Then, in Section V.A, we apply single objective algorithms to optimize the cost, efficiency, and power output of the TMG individually. Next, in Section V.B, we optimize cost, power output, and efficiency simultaneously with a multi-objective GA. We eventually propose our suggested TMG design in Section V.C. We conclude the paper and discuss next steps in Section VI.

## III. Problem Formulation

The problem of optimizing a TMG is put into a standard framework which is outlined below [14].

$$\begin{aligned} &\min \mathbf{J}(\mathbf{x}, \mathbf{p}) = [J_1, J_2, J_3]^\mathsf{T} \\ &\mathbf{x} = [x_1, ..., x_5]^\mathsf{T},\ \mathbf{p} = [p_1, ..., p_m]^\mathsf{T} \\ &x_{i,LB} \leq x_i \leq x_{i,UB}, \quad i = 1, 2, ..., 5 \\ &\text{s.t.} \quad \mathbf{g}(\mathbf{x}, \mathbf{p}) < 0,\ \mathbf{g} = [g_1, g_2, g_3]^\mathsf{T} \end{aligned} \tag{1}$$

Here the objective functions, $J_1, J_2, J_3$, respectively represent *overall power output of the system*, *overall efficiency of the system*, and *overall cost of the system*. The design variables $\mathbf{x}$ in Table 1 represent geometric quantities and are defined as $\mathbf{x} = [x_i]^\mathsf{T} = [w_{yk}, h_{yk}, h_A, h_{pm}, w_{gap}]$, meaning *the width of the yoke*, *the height of the yoke*, *the height of the active materials*, *the height of the permanent magnet*, *the width of the gap*, respectively. For reference on these variable and the overall structure of the device, look to Figure 2. The parameters, $\mathbf{p}$, are largely representing the material properties of different parts in TMG. Some of them are embeded in COMSOL Multiphysics® as system settings for simulations. We refer to the COMSOL® library for further details. The lower and upper bounds ($x_{i,LB}$ & $x_{i,UB}$) are 0.01 and 0.5, respectively. The geometric constraints are all inequality constraints, as indicated in Table 2. Note that unless specifically specified, all the units in the problem formulation are in SI Unit.

We here consider a full thermo-magnetic system which has a thermal cycle given by the time it takes to heat up and cool down the active material. The thermo-magnetic generator furthermore has a power output which is taken from the change in total magnetic flux streaming through the active material, around which the coil is wrapped, so that a current is induced electromagnetically.

The power output is taken as the energy produced over one thermal cycle through the change in this magnetic flux divided by the time it takes for the thermal cycle to come to completion. The efficiency is the total power produced during a thermal cycle divided by the heat energy that has been put into the system and thus, *consumed*. The heat energy is taken with respect to the ambient temperature and is thus the exergy loss over a thermal cycle. The total cost of the system is taken as the volumetric sum of all the material that has gone into the device, weighted by the volumetric cost of each type of material, i.e. the expense required to procure all the material for the device.

As illustrated in Figure 2 the green bar is the active material, the dark blue one is the permanent magnet, and the grey ones are yoke. This figure defines 5 design variables, A physical model with adaptive geometry has been programmed, so these always align. Throughout the project, different constraints have been considered, and some of them have been relaxed or removed. In the original problem formulation, 4 constraints, $\mathbf{g}(\mathbf{x}, \mathbf{p}) = [g_i(\mathbf{x}, \mathbf{p})]^\mathsf{T}$ , are considered,

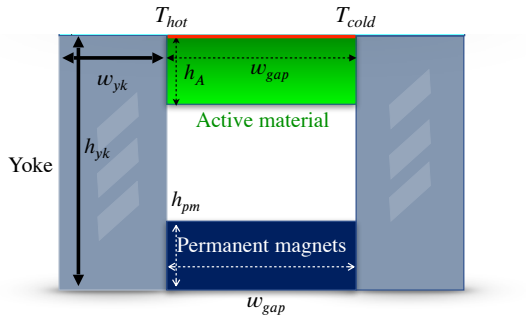


**Fig. 2 The TMG design in our 2D numerical simulation. The green block is the active material; the dark blue is the permanent magnet; the grey ones are the yoke. The red bar on top signifies a *boundary condition on the temperature field*. During heating, it is "turned on", and is given by $T_{hot}$. During cooling it is "turned off" and is given by $T_{cold}$. The latter temperature also defines the boundary condition at all other outer boundaries of the configuration. Not that $p = 0[\text{atm}]$ is set as the reference pressure.**

| Constraint ID | Type | Bound |
|---|---|---|
| *Maximum device height* | Inequality Constraint | $h_{yk} - L_{\max} < 0$ |
| *Maximum device width* | Inequality Constraint | $\left(2 \cdot w_{yk} + w_{gap}\right) - L_{\max} < 0$ |
| *Maximum device volume (eventually removed)* | Inequality Constraint | $h_{yk} \cdot \left(2 \cdot w_{yk} + w_{gap}\right) - V_{max} < 0$ |
| *No overlap* | Inequality Constraint | $h_A + h_{pm} - h_{yk} < 0$ |

**Table 2 Geometric constraints for the TMG system design optimization.**

summarized in the Table 2.

The *Maximum device height* constraint defines a maximum height of the system, as the maximum distance that the device can span across in the vertical direction, and *Maximum device width* does the same for the horizontal direction. Both of these distances are given by, $L_{max}$, as you could always rotate the device around, meaning that the *weakest link* would always be dominating. Here, we chose a distance of $L_{max} = 0.5$m. The *Maximum device volume* constraint puts an upper bound to the total volume taken up by the system. The device will likely have to fit in based on specific industrial applications, i.e., in a car or in a satellite, and there should thus be a limit to how much volume it can take up. It is the same argument that applies to the bound on the total length of the device in any direction, $L_{max}$. The last constraint, *No overlap*, ensures the integrity of the overall design scheme. It means that the gap in the middle of the structure will never become of *negative* height, which is not physically feasible.

Numerous physical parameters, are embedded in the simulation code in COMSOL Multiphysics®, as shown in

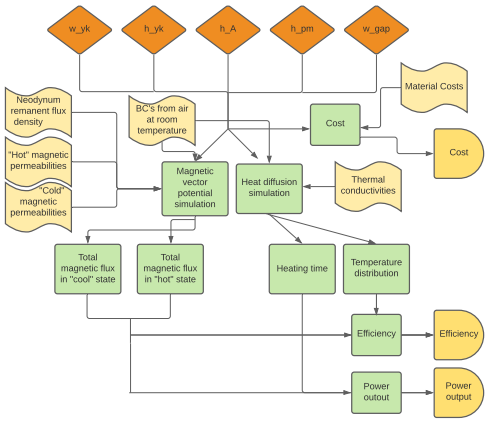


$\mathbf{N^2}$ Diagram

| (x, p) | Geometric design variables, Material cost | Geometric design variables, Thermal parameters | Geometric design variables, Magnetic parameters | | | |
|---|---|---|---|---|---|---|
| | Cost | | | | | Device cost |
| | | Heat diffusion simulation | | Temperature distribution | Heating time | |
| | | | Magnetic vector potential simulation | Total magnetic fluxes | Total magnetic fluxes | |
| | | | | Efficiency | | Efficiency |
| | | | | | Power output | Power output |
| | | | | | | J(x, p), g(x, p) |

**Fig. 3 $\mathbf{N^2}$ and block diagrams for the TMG optimization formulation.**

| Item | Unit | Value |
|---|---|---|
| Magnetic permeability of active material | $[H/m]$ | $4\pi \times 10^{-7}$ |
| Thermal diffusivity of active material | $[m^2/s]$ | $80\pi \times 10^{-7}$ |
| Heat capacity of active material | $[J/(kg \cdot K)]$ | COMSOL® built-in |
| Price of active material | $[\$/m^2]$ | $1.7 \times 10^5$ |
| Magnetic permeability of permanent magnetic | $[H/m]$ | COMSOL® built-in |
| Thermal diffusivity of permanent magnetic | $[m^2/s]$ | COMSOL® built-in |
| Heat capacity of permanent magnetic | $[J/(kg \cdot K)]$ | COMSOL® built-in |
| Flux density of permanent magnetic | [T] | 1.3 |
| Price of permanent magnetic | $[\$/m^2]$ | $1.4 \times 10^3$ |
| Magnetic permeability of yoke | $[H/m]$ | COMSOL® built-in |
| Thermal diffusivity of yoke | $[m^2/s]$ | COMSOL® built-in |
| Heat capacity of yoke | $[J/(kg \cdot K)]$ | COMSOL® built-in |
| Price of yoke | $[\$/m^2]$ | $1.65 \times 10^5$ |
| Initial temperature to heat from | [K] | 300 |
| Final temperature to heat to | [K] | 310 |
| Temperature at the heat source | [K] | 350 |
| Temperature of surroundings | [K] | 300 |

**Table 3 The table for parameters as for the numerical simulations.**

Table 3. They relate to the three types of material used and to the ambient conditions of operation of the device. These four items could be varied, resulting in a change in a multitude of physical properties, which are shown in the table. For an extended project, some of these items could be turned into design variables. Another parameter, which is not shown in the table, is the temperature to which we heat up the active material, taken to be *310 K*. In this project we take the heating process to end once the smallest temperature of the system, is this temperature. This is physically sound as the magnetic permeability will have converged at this temperature, but probably represents a sub-optimal procedure, as there would definitely be some speed to be gained by not requiring that *all* points in the active material has reached this temperature. We also imagine that the device is cooled down to a uniform temperature distribution given by 300K, which does not represent optimal conditions either. For an extended project, these "operating temperatures" could be turned into design variables, and the magnetic permeability could be turned into a scalar field which varies across the geometry. For even more advanced analysis, one could could study the time-dependence of the temperature distribution when the heating and cooling cycles overlap.

## IV. Modeling and Simulation

The multidisciplinary modelling of a system like this is incredibly complex, and the team has undertaken several simplifications and module decouplings to make the simulations run at a reasonable speed. We will repeat the short derivation shown in our second report. The power output $P$ of the system has been determined to be proportional to the total magnetic flux going though the active material raised to the power of two, written as the product of current and voltage:

$$P = IV \tag{2}$$

Assuming the coil around the active material to be completely ohmic, voltage can be decomposed into:

$$V = IR \quad \rightarrow I = \frac{V}{R} \tag{3}$$

substituting Eq. (3) in the Eq. (2) we have

$$P = \frac{V^2}{R} \tag{4}$$

$V$ is induced by the electromotive force of the changing magnetic field. Hence, according to Faraday's law:

$$V = \varepsilon = -N\frac{\Delta\Phi}{\Delta t} \tag{5}$$

The induced current will produce a magnetic field in the opposite direction, according to Lenz's law, which is proportional to $I$, proportional to the change of magnetic flux. We combine this effect with that of the electrical resistance, $R$, and the number of turns, $N$, and throw it all into a constant, $K$. We do not calculate $K$ explicitly, but simply note that the power is proportional to $\Delta\Phi^2 \cdot \frac{1}{\Delta t}$. For optimization, the exact numerical value are not of importance. We express it in "units" of $K$ by simplification: Interestingly, we can optimize our system without ever knowing exactly what the objective function value is.

$$P = K \cdot \Delta\Phi^2 \cdot \Delta t^{-1} \tag{6}$$

The efficiency is taken as, $\frac{E_{out}}{Q_{in}}$, per single cycle. The total heat put into the system (and ejected again), will be taken as $Q_{in} = \int_{\delta V} C_V \cdot (T - 293.15K)\mathrm{d}V$. We simply take the added temperature and multiply with the energy associated with that. This is done for every infinitesimal point in the structure and it is all added together. $C_V$ is kept within the integral, as the different components of the structure have different heat capacities.

$$\begin{aligned}\eta = \frac{E_{out}}{Q_{in}} &= \frac{1}{Q_{in}}\frac{\Delta\Phi^2}{\Delta t} \cdot \Delta t \\ &= \frac{\Delta\Phi^2}{\int_{\delta V} C_V \cdot (T - 293.15K)\mathrm{d}V}\end{aligned} \tag{7}$$

In this derivation, we have stuck with $\Delta t$ and $\Delta\Phi$ for the total change in $t$ and $\Phi$ over half a cycle. $E_{out}$ was thus found simply by multiplying $P$ by $t$. This approach should generalize to incremental changes in $t$ and $\Phi$. Either way, it is clear that the efficiency too can be found to be proportional to a (somewhat) simple expression. This time, we simply get,

$$\eta = G \cdot \frac{\Delta\Phi^2}{\int_{\delta V} C_V \cdot (T - 293.15K)\mathrm{d}V} \tag{8}$$

We decouple the thermal and magnetic modules since a coupled simulation would be extremely time consuming. Here, the incremental inter-dependencies of temperature and the magnetic field during the heating are neglected, as we consider only the extrema of the cycle. We thus only focus on the magnetic permeability of the active material when at its hottest and coldest. It turns out that when we heat from 300K to 310K the active material will transition from being *completely guiding* to *completely non-guiding*. Gadolinium will transition between having the magnetic properties of air to the magnetic properties of iron, which means that we are effectively opening and closing a gap in the "magnetic circuit". To reiterate: having to go all the way between these two extremes over a cycle will likely be sub-optimal, but in this project we are only concerned with optimization of the geometry, and not with how the thermal cycle is carried out. The magnetic module simulations are thus split in two cases - hot and cold conditions for the active material. The difference in total magnetic flux is then computed from these two separate cases. Another module computes all of the thermodynamics: how long it takes for the active material to heat up, so that every point is hotter than the minimum temperature of 310K, and it computes the temperature distribution throughout the device. Combining this data in the separate ways described above, we achieve both expressions for efficiency and for power output. We thus run 2 magnetic simulations and 1 thermal simulation, altogether. The workflow and the decouplings are illustrated in the figure 3, where a block diagram and an $N^2$ diagram are used to illustrated out simulation-optimization loop. Just note that the $N^2$ diagram has abbreviations in it, as it would otherwise fill the entire page.

Validation of the overall model is partly based on the very strong and very clear mesh convergence that has been observed as the model has been run for different meshes (as in Figure 9 in Appendix). It is also based on the validity of the intermediate results, which appear *bullet-proof*. The magnetic field lines, as shown in Figure 4, are in the same numerical scale as those reported by the work of Waske *et al.* [5], and the strength of the magnetic field is at all points in space are comparable to that in the permanent magnet. The heating times ($t = 243.8s$) are reasonable too and the shape of the temperature distribution is exactly as we would expect from the heat equation, as seen in Figure 4. Also, we neglected the inductance of the coils and thus are not able to get any absolute values, as was described previously. In conclusion, we are very confident in our models ability to capture the overall trends that are important for the TMG optimization, but we are also aware that model improvement - especially when it comes to the time and space dependence of the magnetic permeability in the active material, and the inductance of the coil, *which has had no*

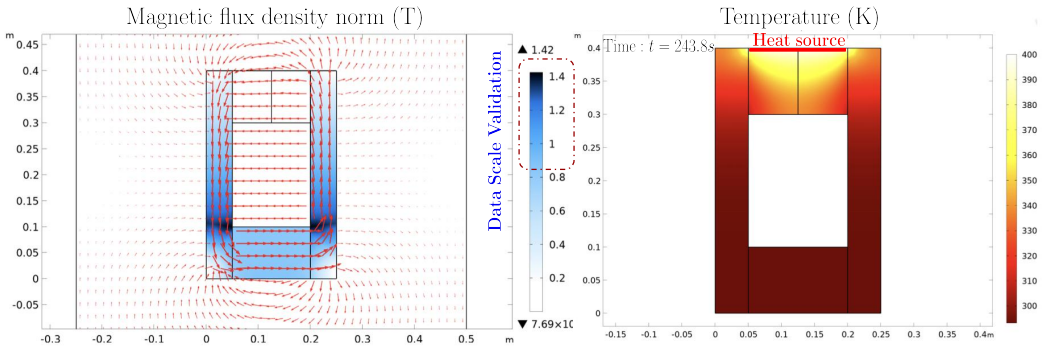


**Fig. 4 Results of a sample simulation of both magnetic and thermal fields. They coincide with physical expectations.**

*physical impact in our model* - could improve the optimization too. There is no literature that reports efficiency and power output in TMG's where the number of coil-turns approaches zero - which could otherwise have been used. As this is an emerging field, there is no literature to compare with for the final results and the variation of these with geometry.

The model is built in COMSOL Multiphysics® using adaptive geometry and adaptive meshes. Despite this, computation times per simulation varied quite a lot, and could be anywhere from 10s and 5min. The mesh was adaptive, so it is not because that larger structures have a lot more finite elements to go over. The magnetic simulations are all computed independently of time, and the computation time is thus the same for them; however, the thermal module is time-dependent, and if the active material becomes very thick and and the yoke very wide, then the heating time will increase non-linearly and extremely fast, as can be seen by solving the 2-dimensional heat-diffusion equation with the boundary conditions of a constant point source (which is the situation we get if the width of the active material is very small compared to the widths of the yoke*). Just as the space step (the mesh) was adaptive, the time step could have been made adaptive too. Unless sacrificing accuracy however, the devices that have longer heating times will inherently also have longer computation times†. For optimization purposes, a link between MATLAB and COMSOL® was established such that a MATLAB script could vary the design variables, feed it into COMSOL®, and get the efficiency, the power output, and the total system cost in return. This procedure was used to get the function evaluations required in the optimization algorithms that have been applied.

## V. Optimization

Genetic algorithm (GA), a heuristic optimization method, was employed to optimize the TMG system to compute multi-objective system optimization. GA's mimic the Darwinian theory of survival of the fittest in nature [17]. The main reason for choosing a GA are: (1) GA's do not require complex problem formulations for specific problems, which makes them easy to implement [18]. (2) GA's work well in scenarios where other methods may have difficulty traversing a complex design space. (3) Because we are searching for a strong design to prove the concept of a computationally optimized TMG design, we do not need to guarantee a global optimum. We aim to produce a strong design on which further experimentation can be based. The following sections detail our optimization process to arrive at a final design recommendation.

### A. Single-objective optimization

Single objective optimization began with a full factorial design of experiments exploring the power, efficiency, and cost objectives. We set a lower bound of 0.05 m and an upper bound of 0.45 m. Using a step size of 0.05 m, a design vector was created for every combination of our five design factors. After applying geometric constraints to the set, we evaluated each objective function for a total of 68 design vectors.

*this turns the problem from one effectively in 1D to 2D, which makes heating time increase much stronger with the thickness of active material

†unless using a combined numerical and analytical approach perhaps, like solving in the form of a discrete Fourier Transform

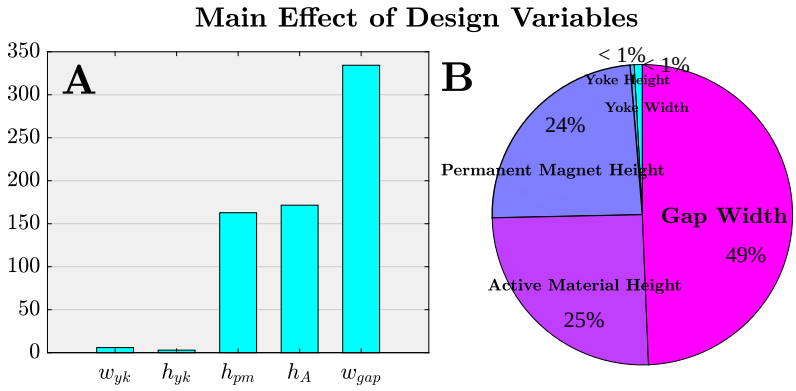


**Fig. 5 The graph representing each effects for design variables for cost module. Subfigure A is the bar plot for effects and B is the pie chart.**

$$
\begin{aligned}
&\min \mathbf{J}(\mathbf{x}, \mathbf{p}) = J \\
&\mathbf{x} = [x_1, ..., x_5]^\mathsf{T}, \ \mathbf{p} = [p_1, ..., p_m]^\mathsf{T} \\
&x_{i,LB} \leq x_i \leq x_{i,UB}, \quad i = 1, 2, ..., 5 \\
&\text{s.t.} \quad \mathbf{g}(\mathbf{x}, \mathbf{p}) < 0, \ \mathbf{g} = [g_1, g_2, g_3]^\mathsf{T}
\end{aligned}
\tag{9}
$$

From the resulting evaluations we computed the variable levels of greatest effect for each objective, shown in Figure 10, in the Appendix. The design of experiments (DoE) gives us a reference frame to compare our final optimizations against. The DoE were also used to help validate optimization algorithms run for each objective by providing the algorithms with an initial guess selected from Figure 10, in the Appendix.

Next, we began true single objective optimization. After constructing a framework allowing MATLAB to interface with COMSOL® models, manipulate their variables, and evaluate results, objectives were evaluated using a SQP gradient based algorithm. We selected gradient based optimization methods to start with because our design space is continuous by nature. All design variables represent geometric dimensions in meters and can be adjusted to any level satisfying all constraints within our defined bounds. The cost function proved easy to optimize with each run taking less than one second. The algorithm consistently converged on the smallest possible design vector which satisfied all constraints with a *first-order optimality measure* of $1.426149 \times 10^{-10}$. This could also be verified through physical intuition about the system geometry. Gradient methods are well suited for our cost objective because cost is a simple algebraic function of cost rates and component areas. We performed a sensitivity analysis on the cost optimization to learn more about our system and verify that the behavior is as expected. Figure 5 shows the main effect of each design variable on the cost objective. Individually, the active material and permanent magnet are by far the most expensive components of the system. We observe that gap width is the greatest driving factor of cost. This makes sense because when gap width changes, either or both of active material height and permanent magnet height must necessarily also change. Therefore, the effect of gap width is equal to the sum of the effects from active material height and permanent magnet height.

The team moved on to optimizing power and efficiency, which proved to be much more complex. Using the same SQP algorithm as for cost, the team found optimized design vectors for the two COMSOL® based objectives. However, the results of each gradient algorithm run were inconsistent. Each run took approximately 15 minutes to execute, and only by selecting the best result from 30 runs did the team observe consistent results. This is likely due to both the complex nature of the power and efficiency functions as well as limitations with the COMSOL® models themselves. To save time in each function evaluation, the mesh resolution was decreased as much as possible and a minimum time step was set. Some function evaluations with very small geometries may have experienced issues due to the minimum COMSOL® time step for temperature integration. When run with initial design vectors from the DoE, the SQP algorithm for power and efficiency tended to get "stuck" without exploring enough of the design space to improve the result. We believe that for any initial guess, the gradient-based method would tend to get stuck in sub-optimal "pits" across the design space, which due to the extremely complex nature of the problem showed a high density of local minima. This density follows from the many interacting and non-linear effects with varying geometry. The behavior of

| | |
|---|---|
| CrossoverFcn | @crossoverheuristic, ratio = 1.3 |
| FunctionTolerance | 1 |
| PopulationSize | 35 |
| CrossoverFraction | .7 |
| MaxStallGenerations | 4 |
| eliteCount | 1 |

**Table 4 Table for hyperparameters of the single objective GA optimization.**

| | |
|---|---|
| CrossoverFcn | @crossoverheuristic, ratio = 1.2 |
| FunctionTolerance | 1e-4 |
| PopulationSize | 100 |
| MaxStallGenerations | 2 |

**Table 5 Table for hyperparameters of the triple objective GA optimization.**

the magnetic field and the heat transfer are fundamentally different in nature and are extremely non-linear. The ability to "guide magnetic flux" can be understood intuitively but can be highly unpredictable from a mathematical point of view where it is not to say how much of an influence a certain change in geometry will really have. As the total magnetic flux furthermore needed to be squared, and the heating times tended to blow up for certain geometries, a highly complex design space is produced, where local minima will likely be *very far away* from the global minimum, and very far away from each other.

Genetic algorithms were found to behave much more consistently for the power and efficiency objectives. Each algorithm was run using the non-default hyperparameters shown in Table 4. A large population was not required to achieve reasonable performance. To avoid getting "stuck" in one area of the objective function, the crossover fraction was reduced to 0.7 so that more population members would be randomly generated. An elite count of two assists the best of those randomly generated members in surviving if they perform well enough. The crossover ratio is set to 1.3 - this parameter did not have a significant effect on the algorithm's performance but is included as a non-default hyperparameter. Function tolerance and maximum stall generations dictate the algorithm's run time by setting the stopping condition. The script will halt optimization when average change in fitness function divided by maximum stall generations is less than function tolerance.

Figure 11 in Appendix shows comparisons of the geometry suggested by the DoE and the geometry suggested by optimization algorithms. Cost shows the smallest possible design vector in each case. Power exhibits different final performance values, but we observe that the overall form of the geometry is the same. Efficiency does not appear as similarly, likely due to the limitations of the DoE method: A step size of 0.05 m overlooks many valid design vectors, while the optimization algorithms have no minimum step size.

### B. Multi-objective optimization

After successfully implementing optimization algorithms for each of the TMG's individual objectives, the team worked to combine all objectives into one genetic algorithm based optimization. We explored gradient based options initially, but their inconsistency across individual runs yielded poor results in the MDO scenario. The team opted to use a heuristic method for the three objective optimizations to reduce complications due to inconsistency. We also removed the non-linear constraint, *Maximum device volume*, which slowed things down unnecessarily due to its nonlinear nature. When run with nonlinear constraints, the genetic algorithm in MATLAB will perform many more function evaluations instead of just one per population member in each generation. Effectively, we still have a maximum volume through the bounds on the variables. Anyway, we first explored a genetic algorithm to optimize cost only to verify that it would behave as expected, as a gradient-based method had previously been used to optimize cost. Although the cost GA was not perfectly consistent, it did successfully find the global optimum many times during our testing. Because we already established more complicated issues with applying gradient methods to the power and efficiency objectives, a multi objective genetic algorithm was a clear choice for our problem due to its compatibility with our objectives and ease of implementation. The multi objective optimization ran using the non-default hyperparameters shown in Table 5.

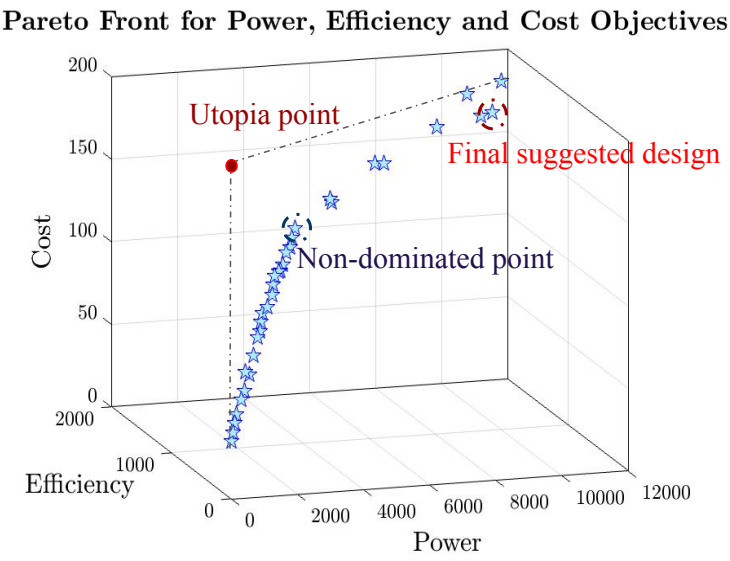


**Fig. 6 The Pareto front for triple objective optimization for cost, power output, and efficiency.**

In selecting hyperparameters for the algorithm, we had two main objectives in mind. First, we wanted to find enough points along the Pareto front to easily visualize the geometric changes between each non-dominated point. Second, we needed to the total run time to not exceed 12 hours so that at least one attempt could be made each day while adjusting algorithm hyperparameters or model settings to increase the algorithm's effectiveness. We found that using a larger population size was the easiest way to increase the population density along the Pareto front, and settled on 100 as a balance between high density and increasing run time. We used the same crossover function as for our single objective optimization because we had previously observed good behavior with it. The other parameters are function tolerance and stall generations, which dictate the stopping conditions for the algorithm. When the geometric average of the Pareto front spread across all generations divided by maximum stall generations is less than the function tolerance, the algorithm will halt further optimization. With this in mind, we adjusted function tolerance and max stall generations to achieve a run time of approximately eight hours for the multi objective optimization to create the Pareto front shown in Figure 6.

The Pareto front generated by the multi-objective algorithm exhibits an obvious turning point in its *slope* near the utopia point where both power and efficiency begin to increase at a heightened rate. One would expect a three objective Pareto front to show a surface rather than a line. We find that efficiency is strongly correlated with power. As a result, our Pareto front takes the "line" appearance. Looking closely at the three dimensional figure in MATLAB, separation between all points is observed. That power and efficiency go along was to be expected. They both scale with square of the total magnetic flux. This made it extremely difficult to *resolve* the Pareto front, such that optimization could be carried out where the additional weight put on one objective would in fact lead to a sub-optimum for the other objective. This results in the *line* nature of the 3D Pareto front, which should otherwise have been a surface. As power output and efficiency move together, the number of degrees of freedom is effectively reduced from 3 to 2, and we go from a surface (3D) to a line (2D). As mentioned though, a little bit of separation is achieved between points in the efficiency - power output - plane. To get a smooth surface however, the optimization would have to be fine tuned - most likely at the heavy expense of computation time.

Note that while cost is directly measured in units of dollars " per distance into the page" for our two dimensional design, efficiency and power are unitless and multiplied by the reparametrization factor $K$ described in Equations (6) and (8). This explains why efficiency in particular is not within the traditional range of [0, 1]. The team created a supplementary animation (can be accessed through `https://hanfengzhai.net/file/finalFront.gif`) to show the relative performances of each objective value and the associated geometry for each point along the Pareto front.

### C. Final suggested design

The final selected design is indicated on Figure 6. Although the selected vector is far from the utopia point, we must consider value and practicality factors in the decision. Figure 7 shows a value based analysis of each point along the

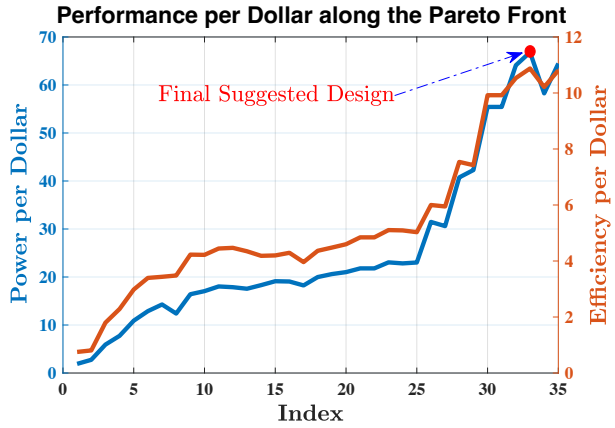


**Fig. 7 The final suggested design based on triple-objective optimization. Note that the selected design has the highest power output per cost and highest efficiency per cost. Green represents the active material, red represents the permanent magnet, and black represents the yoke.**

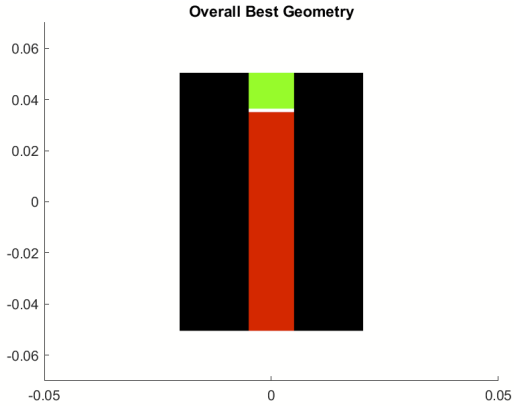


**Fig. 8 The final suggested design based on triple-objective optimization. Note that the selected design has the highest power output per cost and highest efficiency per cost. Green represents the active material, red represents the permanent magnet, and black represents the yoke.**

Pareto front.

As power and efficiency increase, so does performance per dollar. We observe that at the Pareto front's turning point there is a distinct increase in the trend rate of performance per dollar. This curve may have an optimal point outside of our constrained design space. Considering the practicality of our final design, we return to the overall goal of our thermo-magnetic generator: The device should convert heat energy into usable electrical energy. If used to recapture waste heat in an engineering environment, it stands to reason that achieving the highest efficiency possible may tip the scales of the value proposition offered by implementing the device. Although we do not at this stage know the true efficiency of the device, we do know that along our Pareto front the most efficient design is more than 75 times more efficient than the least efficient design. Based on this observation we assume that most of our computed non-dominated points would not be practical enough to use in the real world. Thus, we select the geometry displayed in Figure 8 with the following design variable levels: $[w_{yk}, h_{yk}, h_{pm}, h_A, w_{gap}] = [0.0152, 0.1009, 0.0855, 0.0140, 0.0100]$. The corresponding objectives are Cost = \$167.71, Power output = 11205, Efficiency = 1832.6. (unitless, corresponds to Eqs. (6) and (8)).

## VI. Summary and Future Works

Converting waste heat into usable energy format has a huge potential and market yet lack of applications and studies in the current age. Such form of clean energy can be dated back to Tesla [6]. We investigate the design of a TMG

system that could achieve such a goal. The TMG system contains a permanent magnet, active material, and yoke that converts heat into electricity. In this project, numerical simulations have been carried out to solve an MDO problem that aims to minimize the system's cost, maximize the energy output and maximize the efficiency. The design variables are geometric variables that describe the shape of the TMG. Three geometric constraints were encoded to the optimization process and the parameters were embedded in the simulations in COMSOL Multiphysics®. There are in total three modules for the MDO problem: thermal, magnetic, and cost, coupled with each other to pass on geometric variables. In the actual simulation-optimization loop we decoupled the simulation modules for faster run. We chose genetic algorithm as heuristic methods are easy to tune and apply to complex problems for optimizing the TMG. Both single objective and multi-objective optimizations were carried out and estimated. Design of experiment for single objective optimization on cost suggest width of the gap contributes most for the optimization. Two different designs were proposed based on the single objective optimization on cost and power. Multi-objective GA was applied to optimizing both cost, power output and efficiency of the TMG. During our optimization, we observe that heuristic methods, specifically GA, display good adaptation to our system but admittedly gradient-based methods converge faster. We eventually proposed our suggested design regarding power per cost and efficiency per cost, given by the design vector,

$$[w_{yk}, h_{yk}, h_{pm}, h_A, w_{gap}] = [0.0152, 0.1009, 0.0855, 0.0140, 0.0100] \tag{10}$$

The proposed optimization solution for TMG may guide clean technologies industry for development of TMG. In the future, to proffer a more comprehensive design, we wish to apply the meshing of the whole TMG geometry as the design variables and establish 3D models if possible. Spending more time tuning our algorithms and allowing them to run for longer periods may expose better performing designs. Further, we could perform a new design of experiments with more broad bounds to illuminate an optimal scale for the device, then perform further optimization around that scale. The proposed device design could potentially be implemented to vehicle systems, aerospace industries, campus energy converters, etc. Further exploration of a more advanced design space will help identify engineering systems for which the thermo-magnetic generator is most valuable.

# Appendix

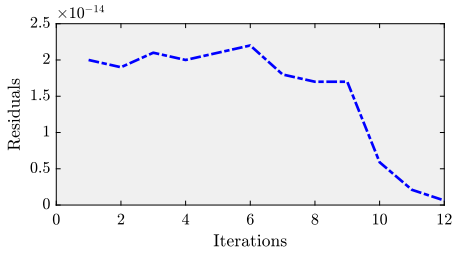


**Fig. 9 The residual convergence plot for TMG numerical simulation in COMSOL Multiphysics®.**

| Variable | Objective | Level | Normalized_Effect |
|---|---|---|---|
| "w_yk" | "cost" | 0.15 | -1.5737 |
| "h_yk" | "cost" | 0.15 | -1.3385 |
| "h_pm" | "cost" | 0.05 | -0.66012 |
| "h_A" | "cost" | 0.05 | -0.70665 |
| "w_gap" | "cost" | 0.05 | -1.7706 |
| "w_yk" | "power" | 0.05 | 0.18508 |
| "h_yk" | "power" | 0.45 | 0.7413 |
| "h_pm" | "power" | 0.25 | 2.0658 |
| "h_A" | "power" | 0.15 | 0.26235 |
| "w_gap" | "power" | 0.15 | 0.32028 |
| "w_yk" | "efficiency" | 0.05 | 0.40488 |
| "h_yk" | "efficiency" | 0.45 | 1.4862 |
| "h_pm" | "efficiency" | 0.25 | 1.7284 |
| "h_A" | "efficiency" | 0.15 | 0.36649 |
| "w_gap" | "efficiency" | 0.05 | 0.74251 |

**Fig. 10 Table showing variable levels of greatest effect from the DoE. All effects have been normalized to the same scale within each respective objective.**

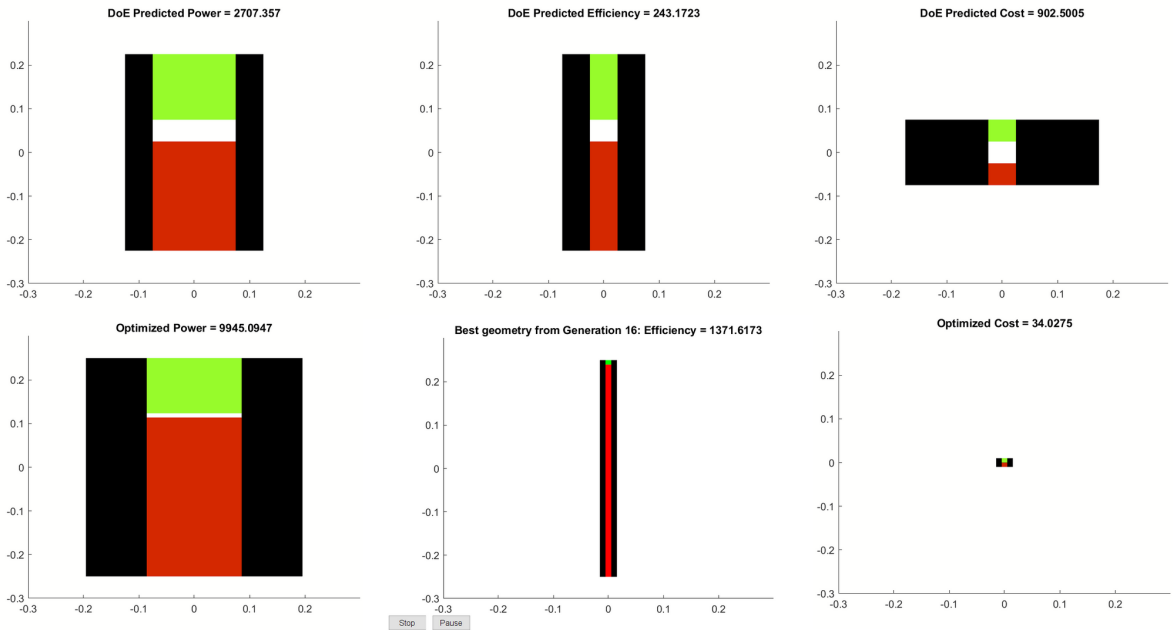


**Fig. 11 Best geometry comparison between DoE and single objective optimization methods**

# References


[1] Rowe, A.M. A new twist. Nat Energy 4, 12–13 (2019). https://doi.org/10.1038/s41560-018-0307-9.

[2] U.S. Energy Information Administration. Wind explained: Electricity generation from wind. URL: https://www.eia.gov/energyexplained/wind/electricity-generation-from-wind.php#:~:text=Electricity%20generation%20with%20wind&text=Total%20annual%20U.S.%20electricity%20generation,U.S.%20utility%2Dscale%20electricity%20generation.

[3] Battery Market Size, Share & Trends Analysis Report By Product (Lead Acid, Li-ion, Nickle Metal Hydride, Ni-cd), By Application (Automotive, Industrial, Portable), By Region, And Segment Forecasts, 2020 - 2027.

[4] World Energy Needs and Nuclear Power. World Nuclear Energy Association. URL: https://world-nuclear.org/information-library/energy-and-the-environment/nuclear-energy-and-sustainable-development.aspx

[5] Waske, A., Dzekan, D., Sellschopp, K. et al. (2019) Energy harvesting near room temperature using a thermomagnetic generator with a pretzel-like magnetic flux topology. Nat Energy 4, 68–74.

[6] Tesla, N. Thermomagnetic motor. US Patent 396,121 (1889).

[7] Edison, T. A. Pyromagnetic generator. US patent 476,983 (1892).

[8] Schierning, G. Bring on the heat. Nat. Energy 3, 92–93 (2018).

[9] U.S. Department of Energy, Energy Information Administration. 2014. Annual Energy Outlook 2014: Industrial Sector Key Indicators and Consumption.

[10] O. Gutfleisch, M. A. Willard, E. Brück, et al. Magnetic materials and devices for the 21st century: stronger, lighter, and more energy efficient. Advanced Materials, vol. 23, no. 7, pp. 821–842, 2011.

[11] U.S. Energy Information Administration. Electricity explained: Magnets and electricity. URL: https://www.eia.gov/energyexplained/electricity/magnets-and-electricity.php

[12] Kittel, C. (1986) Introduction to Solid State Physics. John Wiley & Sons. ISBN 0-471-87474-4.

[13] Bidwell, Shelford (1911). "Magnetism". In Chisholm, Hugh (ed.). Encyclopædia Britannica. 17 (11th ed.). Cambridge University Press. pp. 321–353.

[14] Agte, J., de Weck, O., Sobieszczanski-Sobieski, J., Arendsen, P., Morris, A., & Spieck, M. (2009). MDO: assessment and direction for advancement—an opinion of one international group. Structural and Multidisciplinary Optimization, 40(1-6), 17–33.

[15] Dan'kov, S. Y., Tishin, A. M., Pecharsky, V. K., & Gschneidner, K. A. (1998). Magnetic phase transitions and the magnetothermal properties of gadolinium. Physical Review B, 57(6), 3478–3490.

[16] COMSOL Inc. LiveLink for MATLAB User's Guide. URL: https://doc.comsol.com/5.4/doc/com.comsol.help.llmatlab/LiveLinkForMATLABUsersGuide.pdf.

[17] Katoch, S., Chauhan, S.S. & Kumar, V. A review on genetic algorithm: past, present, and future. Multimed Tools Appl 80, 8091–8126 (2021).

[18] Genetic Algorithms | Advantages & Disadvantages. URL: https://electricalvoice.com/genetic-algorithm-advantages-disadvantages/.

[19] Houssem Rafik El Hana Bouchekara, Afef Kedous-Lebouc, and Jean Paul Yonnet, "Electromagnetic Design of a Magnetic Field Source for a Magnetocaloric Refrigerator," Progress In Electromagnetics Research M, Vol. 19, 251-263, 2011.